Available online at www.sciencedirect.com
SCIENCE DIRECT®
Journal of Sound and Vibration 279 (2005) 557–579
JOURNAL OF SOUND AND VIBRATION
www.elsevier.com/locate/jsvi

Variability of the coupling loss factor between two coupled plates

W.S. Park, D.J. Thompson*, N.S. Ferguson

Institute of Sound and Vibration Research, University of Southampton, Highfield, Southampton SO17 1BJ, UK

Received 9 January 2003; accepted 11 November 2003

Abstract

Within statistical energy analysis (SEA), the coupling loss factor (CLF) is a statistical quantity defined in terms of the average behaviour of an ensemble of similar systems. Thus, the 'effective' CLF for a given realization may differ from the ensemble average. The effective CLF of two coupled plates with low modal density and low modal overlap fluctuates significantly compared with the ensemble average CLF. Accordingly, the CLF is the main parameter expected to determine the confidence intervals in the SEA prediction. The aim of the present paper is to quantify the variability of the effective CLF for the case of two finite rectangular plates. Extensive parameter investigations have been performed by using the dynamic stiffness method (DSM) and a 'numerical' power injection method (PIM) using the SEA power balance equations. The effects of frequency bandwidth and the number of modes in a band were separated by using frequency averages at a series of constant bandwidths rather than one-third octave averages, while the modal overlap is made independent of frequency by setting the damping loss factor to be inversely proportional to frequency. Finally, an improved empirical model for the variability of the CLF is derived, from these numerical results, in terms of the modal overlap factor and the number of modes in a frequency band. This model can subsequently be used to evaluate the uncertainty of the CLF of such a system.

1. Introduction

Statistical energy analysis (SEA) has become quite widely used for studying the vibro-acoustic behaviour of structures, vehicles, ships and buildings at high frequencies [1–4]. Whereas traditional deterministic methods such as the finite element method (FEM) give a detailed analysis of the behaviour of one typical structure, SEA gives a broad estimate of the average response of a

*Corresponding author. Tel.: +44-23-8059-2510; fax: +44-23-8059-3190.
E-mail address: djt@isvr.soton.ac.uk (D.J. Thompson).

0022-460X/$ - see front matter © 2004 Elsevier Ltd. All rights reserved.
doi:10.1016/j.jsv.2003.11.035

notional ensemble of similar structures [5]. However, despite its name, SEA does not normally provide any statistical information on the likely distribution of the behaviour of a given realization within this ensemble. Particularly at the lower end of its frequency range of application, where both the modal overlap and the number of modes in a frequency band tend to reduce, the behaviour of a given member of the ensemble may differ considerably from the average behaviour predicted by SEA. If this inherent uncertainty can be quantified, SEA predictions can be used meaningfully at these lower frequencies, albeit with a wide confidence interval.

Lyon and DeJong [5] gave estimates of the variance of coupling loss factors (CLFs) and of the response of a subsystem, based on mode shape functions. However, these formulae are rather difficult to use and have not found wide application. Moreover, it was shown by Craik et al. [6] that they tend to over-estimate the variation found in typical building structures. An alternative approach was developed by Craik et al. [6] from observing that the distribution of the effective CLFs for individual realizations relative to the ensemble average was similar to the distribution of the point mobility of the receiver subsystem relative to its characteristic mobility. The variation in mobility is derived from expressions given by Skudrzyk [7]; see also Moorhouse and Gibbs [8]. Whilst this approach to CLF variability is not rigorous, it provides a practical approach. However, it has the limitation that no estimates of variability are given when the modal overlap exceeds unity.

Fahy and Mohammed [9] studied the effects of random geometric perturbation on power transmission in coupled beams and plates using analytical models. Their results showed that the modal overlap factors of the uncoupled subsystems and the number of coupled modes of the total system are the two main parameters that control the variability in the power flow and the associated CLF. An empirical formula for the normalized variance of the CLF between two coupled plates was given by Mohammed [10], obtained by fitting a curve to analytical results obtained for plates of different lengths.

Confidence intervals for the SEA response estimate were examined by Manning [11]. A couple of sources for the randomness and the variance in SEA predictions were discussed. Hopkins [12] also investigated the confidence limits for the CLF using a perturbation method. The approach was used to calculate the expected range of the response for plate systems with low modal density and low modal overlap. The results in terms of the 95% confidence intervals were seen to provide a satisfactory estimate of the expected range, while the results gave significant underestimates for the minimum values when the receiver subsystem was not directly coupled to the source subsystem.

In this paper, a more extensive parametric study has been performed for two rectangular plates coupled along a common edge. These are represented analytically using the dynamic stiffness method (DSM) [13]. Results are obtained in the form of the effective CLF. The term effective CLF is used here to distinguish the result for a single realization from the true CLF which applies to the ensemble average. CLF estimates are obtained from the dynamic stiffness calculation results by applying the power injection method (PIM) [14] to the numerical response predictions. From the results of these calculations, an 'empirical' model is proposed herein to describe the variance of the effective CLF over a wide range of parameter values. It is shown that the parameters of most importance are the modal overlap factor and the number of modes in the frequency band of the two subsystems. The cases considered have been selected in order to be

able to specify these two parameters independently, as well as varying other parameters over a wide range.

In order to provide an unbiased estimate of the mean CLF for comparison, the ensemble average result of Wester and Mace [15] has been adopted, as it allows for the dependence of the CLF on the damping loss factor (DLF) when the two plates are strongly coupled.

2. Parameter investigation using DSM model

In this study, a number of parameters of the two-plate system are varied, including plate dimensions and damping to investigate the effects on the CLF. It will be shown that two parameters, in particular, affect the variability of the CLF: the average number of modes in a frequency band N and the modal overlap factor M. Usually SEA is considered to be applicable to a frequency band-average analysis if there are several modes in each frequency band (for example, at least 3 [16], 6 [17] or 10 [18] are stated) to ensure that the field is sufficiently diffuse, and the modal overlap factor is at least unity [16–19]. If these conditions are not met, considerable deviations may occur in the results.

The approach adopted in this paper is to separate the effects of these two parameters, and make each of them independent of frequency. The average number of modes in a band will be made independent of frequency by using frequency averages for overlapping bands at a series of constant bandwidths. The modal overlap will also be made independent of frequency by setting the DLF to be inversely proportional to frequency.

However, initially a model with constant DLFs and based on one-third octave frequency bands is considered for illustration purposes.

2.1. Initial model in one-third octave bands

Two coupled rectangular aluminium plates are considered initially, with thickness $h_1 = 3$ mm and $h_2 = 2$ mm, respectively, lengths $L_1 = 0.5$ m and $L_2 = 1$ m, width $b = 1$ m, and equal damping $\eta_1 = \eta_2$, as shown in Fig. 1. To facilitate use of the DSM [13], it is assumed that the two opposite edges along the longitudinal direction, $y = 0$ and b, are simply supported; the other edges are free. To model a harmonic point force applied inside one plate, the source plate is separated into two parts at the longitudinal position of the applied force. Thus this system may be considered to consist of three plates, two directly excited plates and one receiver plate. The global dynamic stiffness matrix of the system is derived by assembling the dynamic stiffness matrix of each plate and applying the compatibility and equilibrium conditions at the joints. In the present model, the in-plane motion of plate is included. Assuming a harmonic point force is applied at a transverse edge, the system may be analyzed by the assembled dynamic stiffness matrix for the system. The system is analyzed for each half-sine order across the width of the plates and each frequency separately. This model has a modal density that is approximately constant with frequency. The modal overlap factor ($M = \eta\omega n(\omega)$) depends on frequency as the DLFs were kept constant in this section. Two values of DLF are used: $\eta_1 = \eta_2 = 0.1$, although rather high for typical structures, ensures that the modal overlap factor does not become too small in the frequency range considered, whereas 0.01 gives a more representative value.

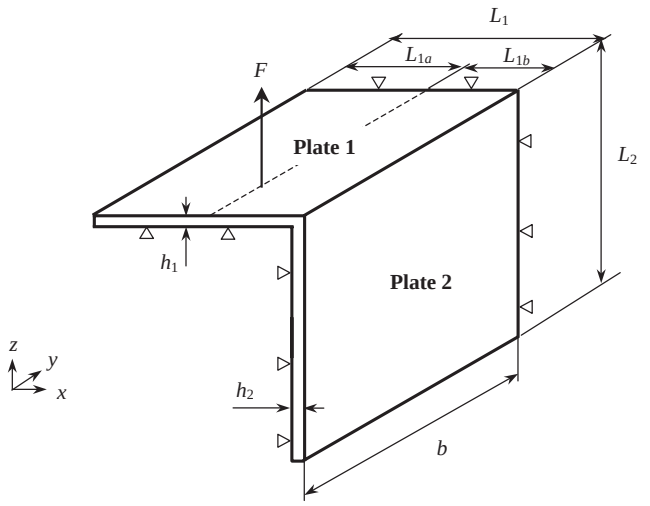

Fig. 1. Two perpendicular plates with a point force F applied inside one plate: width $b = 1.0$ m, length $L_1 = 0.5$ m, $L_2 = 1.0$ m, thickness $h_1 = 3.0$ mm, $h_2 = 2.0$ mm, the DLF $\eta_1 = \eta_2 = 0.1$, material: aluminium (Young's modulus $E = 7.24 \times 10^{10}$ N/m^2, Poisson's ratio $\mu = 0.333$, material density $\rho = 2794$ kg/m^3).

In these calculations the point force is located at a range of different positions to simulate 'rain-on-the-roof' excitation. To simulate this, a total of 400 point forces have been used, applied individually first on plate 1, then on plate 2. For numerical convenience, these were chosen at 20 random y co-ordinates, the same for each of 20 random x co-ordinate positions. All points are chosen to exclude an area around the edge of the plate in order to avoid nearfield effects, although these are inevitable at low frequencies. These forces are all uncorrelated, and are assumed to have an identical broadband spectrum.

The strain energy response of each plate to these forces is calculated and integrated over the plates for each frequency. Equating the dissipated power in the receiver plate to the net power flowing from source to receiver gives

$$\begin{Bmatrix} \omega\eta_2 E_2^1 \\ \omega\eta_1 E_1^2 \end{Bmatrix} = \omega \begin{bmatrix} E_1^1 & -E_2^1 \\ -E_1^2 & E_2^2 \end{bmatrix} \begin{Bmatrix} \hat{\eta}_{12} \\ \hat{\eta}_{21} \end{Bmatrix}, \tag{1}$$

where the superscript indicates the subsystem that is excited, E_1 and E_2 are the total time averaged energies of the two subsystems (approximated by the maximum strain energy in a cycle), η_i is the DLF and $\hat{\eta}_{ij}$ the effective CLF. The energies are calculated for each forcing point, averaged and then summed over one-third octave bands. The matrix is then inverted to yield the effective CLFs.

The results are shown in Fig. 2 for two values of damping $\eta_1 = \eta_2 = 0.1$ and 0.01. These effective CLFs are compared with $\eta_{ij\infty}$, the result derived from the coupling between two infinite plates [17] and $\eta_{ij,ens}$, the ensemble average result from Wester and Mace [15] and given in the appendix. At low frequencies, the ensemble average CLFs are lower than the semi-infinite results $\eta_{ij\infty}$ since the coupling is strong [20] and there is a significant influence of the finite size of the plates and the value of damping in them. At these long wavelengths the production of reflections from the opposite end of the plate from the junction is important and not accounted for in the

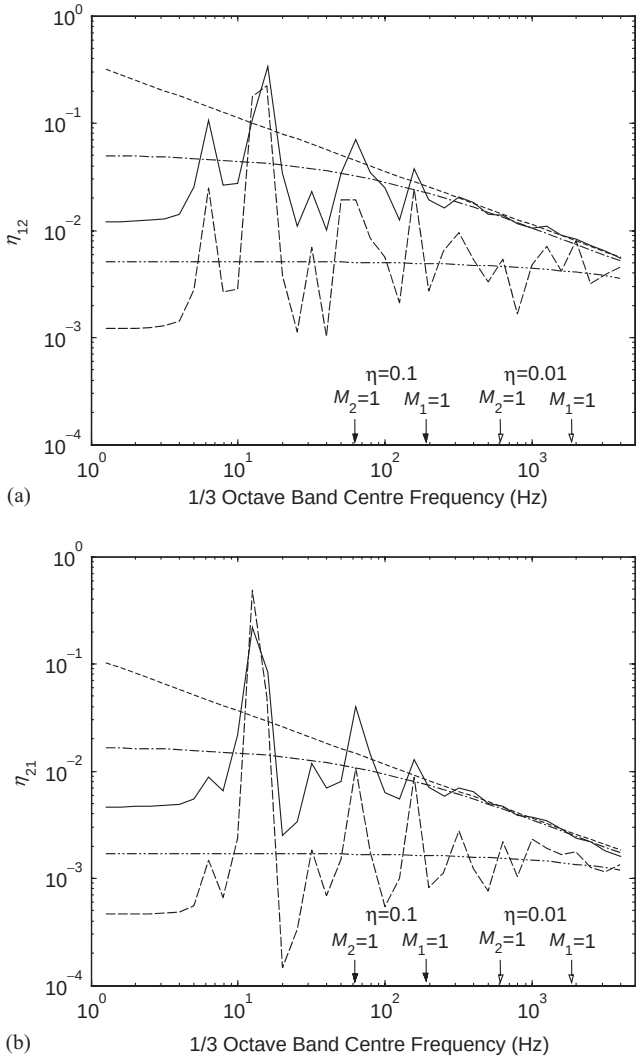

Fig. 2. Various estimates of the CLF, (a) η_{12} and (b) η_{21}, for a two-plate system ($h_1 = 3$ mm, $L_1 = 0.5$ m, $h_2 = 2$ mm, $L_2 = 1$ m, $b = 1$ m, $\eta_1 = \eta_2$, material: aluminium). - - -, CLF for two semi-infinite plates $\eta_{ij\infty}$; — · —, ensemble average CLF $\eta_{ij,ens}$ for $\eta = 0.1$; —, 'effective' CLF $\hat{\eta}_{ij}$ for $\eta = 0.1$; — · · —, ensemble average CLF $\eta_{ij,ens}$ for $\eta = 0.01$; — — —, 'effective' CLF $\hat{\eta}_{ij}$ for $\eta = 0.01$. The arrows indicate frequencies at which the modal overlap factors of the two individual plates equal 1.

semi-infinite plate model. For more highly damped plates the differences between the CLF for the ensemble average and semi-infinite plates are smaller. In the limit, at high frequencies or as damping increases, the effect of reflection from a wave transmitted across the junction into the finite plate will be negligible.

The effective CLFs for numerical realizations fluctuate considerably relative to the corresponding ensemble average CLF result $\eta_{ij,ens}$. As one would expect, the curves all converge closely at high enough frequencies, where the modal overlap becomes high. The frequencies at

which the corresponding modal overlap factors of the individual plate realizations are equal to 1 are indicated in the figure. Below 10 Hz there are no modes at all in the source plate and the use of SEA would not be expected to yield valid results.

2.2. Model with constant modal overlap and constant bandwidth

The modal density and modal overlap factor are related to the geometric and material properties. The modal density of the flexural modes of a uniform isotropic plate is approximately $n(\omega) = 0.276\, S/hc_L$ where S is the surface area, h is the thickness and $c_L = (E/\rho(1-\nu^2))^{1/2}$ is the longitudinal wavespeed in the plate [5]. (It is convenient to introduce the longitudinal wavespeed to simplify the relationship, although the waves do not have any longitudinal contribution.) The modal density is thus proportional to the *area*/*thickness* of the plate and it is independent of frequency. Thus the modal overlap factor M is in general dependent on frequency as well as the geometric and material properties.

In order to generate a system with a constant modal overlap factor for all frequencies, the DLF was chosen to be inversely proportional to frequency, $\eta_1 = \eta_2 = 1/f$ although with a maximum value of 0.3. This variation is not typical, since normally the loss factor is found to be approximately independent of frequency, but as stated, it is introduced here in order to generate a system with a constant modal overlap factor. The number of modes in a frequency band, N, is also made independent of frequency by using constant bandwidths. Consequently, the modal overlap factor and the number of modes in a band are both independent of frequency, so that statistical analyses can be taken across the frequency range considered. Both M and N can also be varied independently of each other.

In this study, firstly, narrow-band energies and powers were calculated for the two-plate system using a DSM model that includes the in-plane motion of the plates. A frequency spacing of 1 Hz was used up to a maximum of 1 kHz. In this model at least one frequency point lies within the half-power bandwidth ηf of each mode. The plate energies were then averaged in overlapping bands with constant frequency bandwidths to provide a continuously varying curve. Bandwidths of 2, 4, 6, 10, 20, 40, 60, 100, 200 and 400 Hz were considered.

The effective CLFs corresponding to the frequency bands $\langle \hat{\eta}_{ij} \rangle$ are obtained from these energies by a numerical PIM experiment as defined in Eq. (1). $\langle\ \rangle$ denotes a frequency-averaged quantity. The frequency-averaged effective CLF results are presented relative to the ensemble average CLF $\eta_{ij,ens}$ of Wester and Mace [15] and given in the Appendix. This is used rather than the CLF derived from semi-infinite plates, $\eta_{ij\,\infty}$, which is biased for strongly coupled subsystems, as shown in Fig. 2.

Fig. 3 shows the effective CLFs and the corresponding ensemble average CLF for the initial model calculated at 1 Hz spacing. This has plate dimensions as in the previous section, but has frequency-dependent damping and no frequency-band averaging. Also shown, are estimates of upper and lower bounds, given by $2/\pi M$ and $\pi M/2$ times the ensemble average result $\eta_{ij,ens}$. These are obtained from the maxima and minima of the mobility given by Skudrzyk [7], as used in the formulae for CLF bounds given by Craik et al. [6]. The bounds in Fig. 3 were generated using the modal overlap factor for either the source plate M_{source} (i.e., M_1 for η_{12} and M_2 for η_{21}) or the receiver plate $M_{receiver}$. It can be seen that the variation in the CLF is greater than that estimated from either of the bounds shown in this case.

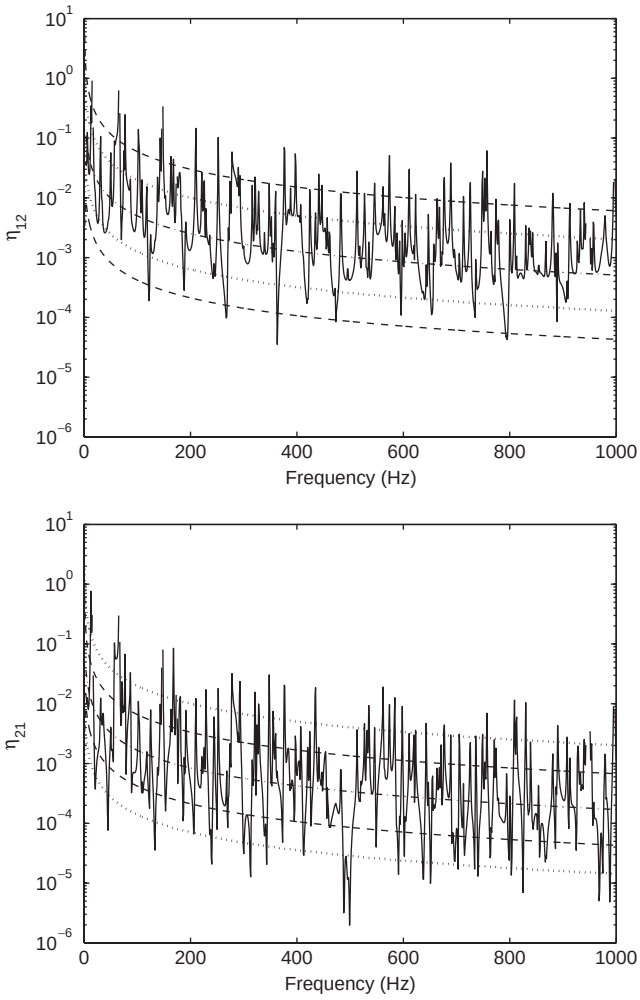

Fig. 3. The effective CLFs $\hat{\eta}_{ij}$, the ensemble average CLF $\eta_{ij,ens}$, and upper and lower bounds from Skudrzyk [7], for the initial model ($\eta = \min(0.3, 1/f)$, $M_1 = 0.053$, $M_2 = 0.16$). —, the effective CLF; – · –, the ensemble average CLF; - - -, upper and lower bounds based on using M_{source}: ....., upper and lower bounds based on using $M_{receiver}$ from Skudrzyk [7].

It is clear that the effective CLF varies considerably relative to the ensemble average result. When plotted on a logarithmic scale, as here, the distribution appears symmetric. In the remainder of the paper the mean is removed by considering the ratio of the frequency-averaged effective CLF to the ensemble average CLF, $\langle \hat{\eta}_{ij} \rangle / \eta_{ij,ens}$ and expressing this in decibel (dB) form. (The ensemble average is used here as it is a more accurate estimate of the coupling loss factor than $\eta_{ij\infty}$). This is shown in Fig. 4 for η_{12} for different frequency bandwidths. The results for η_{21} were found to be similar. Within a given graph the results at different frequencies correspond to the same values of modal overlap and number of modes in a band. This set of results is therefore used as the basis of a statistical analysis. The mean of these results over all frequency bands, along with a range of ± 2 standard deviations (σ) calculated in terms of the dB values, has been

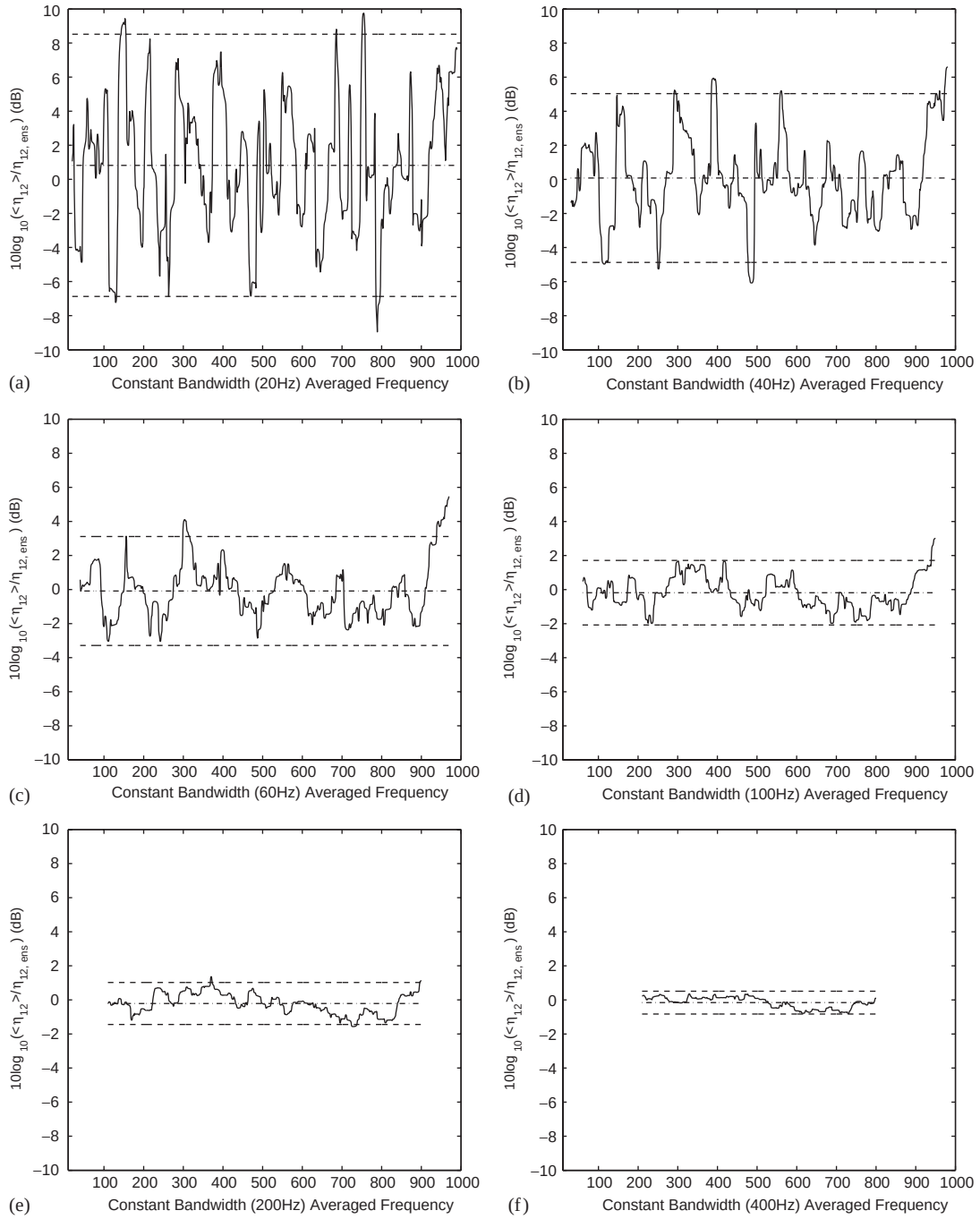

Fig. 4. Bandwidth effect on the mean and ± 2 standard deviations (2σ) of the logarithmic ratio of the frequency averaged effective CLF $\langle \hat{\eta}_{12} \rangle$ to the ensemble average CLF $\eta_{12,ens}$ ($\eta = \min(0.3, 1/f)$, $M_1 = 0.053$, $M_2 = 0.16$). —, $10\log_{10}(\langle \hat{\eta}_{12} \rangle / \eta_{12,ens})$; – · –, $10\log_{10}(\langle \hat{\eta}_{12} \rangle / \eta_{12,ens})_{mean}$; - - -, mean $\pm 2\sigma$ of $10\log_{10}(\langle \hat{\eta}_{12} \rangle / \eta_{12,ens})$. (a) 20 Hz, (b) 40 Hz, (c) 60 Hz, (d) 100 Hz, (e) 200 Hz and (f) 400 Hz bandwidths.

determined and is also shown in each case. Clearly, as the bandwidth increases, the range $\pm 2\sigma$ reduces, whereas the mean is close to 0 dB throughout. As the bandwidth increases, the average number of modes in a frequency band, N_1 or N_2 also increases. This can be obtained from the modal density $n(\omega)$ multiplied by the bandwidth $\Delta\omega$. The upper graph of Fig. 5 shows the values of 2σ for η_{12} from Fig. 4, and the equivalent results for η_{21}, plotted against the average number of modes per band for the corresponding source plate N_{source}. The middle graph shows the equivalent results when plotted against the number of modes per band for the corresponding receiver plate $N_{receiver}$. The lower graph is based on N_{12}, which is a combined number of modes used by Mohammed [10], $N_{12} = \sqrt{N_1 N_2}$, i.e., the geometric mean value of N_1 and N_2. The results of 2σ for η_{12} and for η_{21} show similar levels for a given frequency bandwidth and are simply shifted horizontally by plotting against N_{source}, $N_{receiver}$ or N_{12}. The combined measure N_{12} therefore seems more appropriate as it accounts for both plates in a symmetrical way. This is discussed further in the following section.

In the next section, these numerical results, and others like them, are used to derive an empirical formula for the confidence interval of the effective CLF in terms of the modal overlap factor and the number of modes in a frequency band.

3. Variability of the CLF

3.1. Parameter variation

In this section, a large number of idealizations of the two coupled plates are considered. These are generated by varying several parameters either separately or simultaneously. It is not the intention here to explore the dependence on every possible parameter of the two-plate system. The parameters varied are summarized in Table 1 and discussed below. The actual values of plate thickness, length or width used are also listed below the table.

The main parameters varied are the length of plate 2, its thickness and the width of both plates. These are each varied in logarithmically spaced steps in a range either side of the initial values. However, changing each of these parameters in isolation would lead to changes in the modal overlap factor of plate 2, M_2. The first set of conditions involves changing the length of plate 2 which leads to changes in M_2. However, when the thickness is varied, the length of plate 2 is also varied in order to generate a set of cases with a constant modal overlap factor. Similarly when the width of the plates is varied, both their lengths are adjusted in order to keep the modal overlap factors unchanged. The corresponding dimensions for plate 1 are not varied (except in the third case) as the CLF η_{21} provides the corresponding result for changes in source plate dimensions. In each case, the damping values of the two plates are set to be frequency dependent $\eta \propto 1/\omega$, in order to keep the modal overlap factors constant with frequency. The other parameters are the same as the initial model of the previous section.

Three different levels of damping (high damping $\eta = 10/f$, medium damping $\eta = 3/f$ and light damping $\eta = 1/f$) are also considered, with $\eta_1 = \eta_2$. This provides another way of altering the modal overlap factors. In each case η is limited to a maximum value of 0.3. To investigate the effect of different damping levels for the two plates, whilst keeping the modal overlap factors constant with frequency, calculations have also been performed with the two plates chosen to

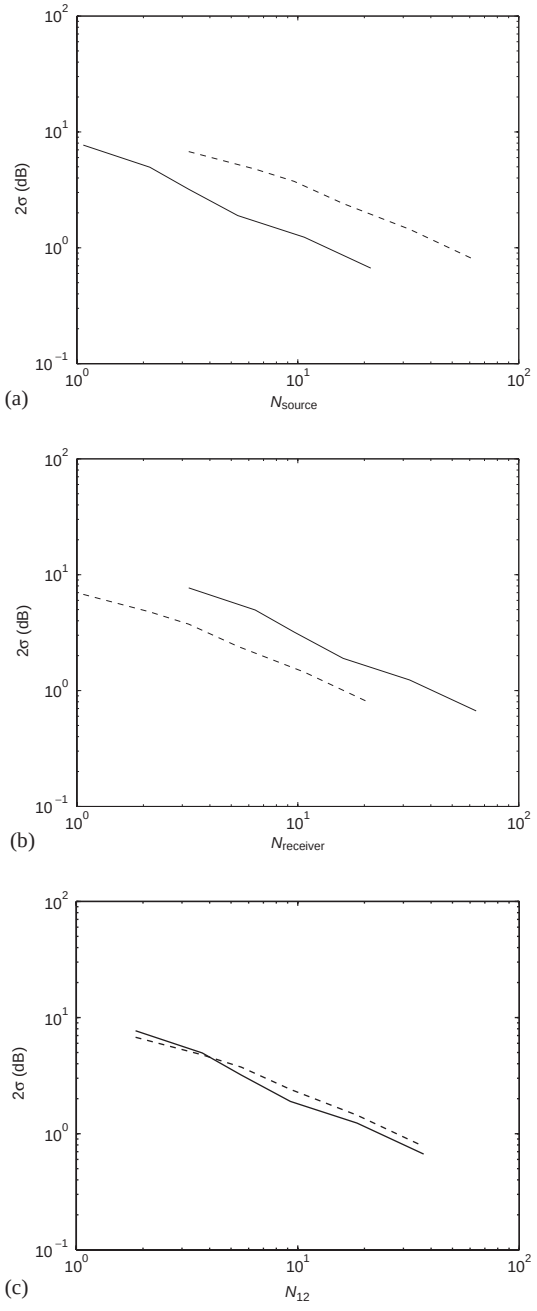

Fig. 5. Two standard deviations (2σ) of $10\log_{10}(\langle\hat{\eta}_{ij}\rangle/\eta_{ij,ens})$ for different frequency bandwidths plotted against (a) N_{source}, (b) $N_{receiver}$, and (c) N_{12}, the geometric mean of N_1 and N_2 ($\eta = \min(0.3, 1/f)$, $M_1 = 0.053$ and $M_2 = 0.16$): —, 2σ for η_{12}; - - -, 2σ for η_{21}.

Table 1
Summary of parameter variations for L-shaped coupled plates

Parameter	Fixed	Varied		M_1	M_2	η_2/η_1
Initial model (h_1= 3 mm, h_2= 2 mm)	L_1,L_2,h_1,h_2,b,η_1,η_2, $n_1(\omega)$, $n_2(\omega)$	—	—	$\propto f$	$\propto f$	1.0
L_1/L_2[a]	L_1,h_1,h_2,b	L_2	$\eta_1 = \eta_2 \propto 1/\omega$	0.53	2.5 ~ 0.32	1.0
h_1/h_2[b]	L_1,h_1,b	L_2,h_2	$\eta_1 = \eta_2 \propto 1/\omega$	0.53	1.6	1.0
L_1/b[c]	h_1,h_2	L_1,L_2,b	$\eta_1 = \eta_2 \propto 1/\omega$	0.53	1.6	1.0
High damping	L_1,L_2,h_1,h_2,b	—	$\eta_1 = \eta_2 \propto 1/\omega$	0.53	1.6	1.0
Medium damping	L_1,L_2,h_1,h_2,b	—	$\eta_1 = \eta_2 \propto 1/\omega$	0.16	0.48	1.0
Light damping	L_1,L_2,h_1,h_2,b	—	$\eta_1 = \eta_2 \propto 1/\omega$	0.053	0.16	1.0
$\eta_1 > \eta_2$	L_1,L_2,h_1,h_2,b	—	$\eta_1 \neq \eta_2 \propto 1/\omega$	0.53	0.48	0.30
$\eta_1 > \eta_2$	L_1,L_2,h_1,h_2,b	—	$\eta_1 \neq \eta_2 \propto 1/\omega$	0.16	0.16	0.33

The variation of η_1 and η_2 subsequently produces constant values of M_1 and M_2.

[a] L_1/L_2: the length of plate 1 (0.5 m) is fixed and the length of plate 2 is varied from 1.58 to 0.20 m (1.58, 1.26, 1.00, 0.79, 0.63, 0.50, 0.40, 0.32, 0.25, 0.20 m).

[b] h_1/h_2: the thickness of plate 1 (3 mm) is fixed and the thickness of plate 2 is varied from 9.49 to 0.949 mm (9.49, 5.99, 4.75, 3.78, 3.00, 2.38, 1.89, 1.50, 1.19, 0.949 mm). The length L_2 is varied simultaneously to ensure constant N_2.

[c] L_1/b: the widths of the two plates are varied from 1.58 to 0.20 m (1.58, 1.26, 1.00, 0.79, 0.63, 0.50, 0.40, 0.32, 0.25, 0.20 m). The lengths of the plates are varied simultaneously to maintain the same areas and hence constant values of N_1 and N_2.

have different levels of damping whilst retaining $\eta \propto 1/\omega$. These were from high to medium damping ($\eta_2/\eta_1 = 0.3$ corresponding to $M_1 = 0.53$, $M_2 = 0.48$) and from medium to low damping ($\eta_2/\eta_1 = 0.33$ corresponding to $M_1 = M_2 = 0.16$). The CLF η_{21} corresponds to the opposite cases, so these are not considered separately.

3.2. Variability of the CLF for finite plates

All the results covering the extensive parameter variations are considered together to establish appropriate parameters to describe the variability of the CLF and to quantify its confidence interval. For example, some results of the logarithmic CLF ratio $10\log_{10}(\hat{\eta}_{ij}/\eta_{ij,ens})$ for two extreme cases among all parameter variations are shown in Fig. 6. These two cases are (a) the shortest and widest (h_1= 3 mm, h_2= 2 mm, L_1= 0.32 m, L_2= 0.63 m, b= 1.58 m) and (b) the longest and narrowest (h_1= 3 mm, h_2= 2 mm, L_1= 2.5 m, L_2= 5.0 m, b= 0.20 m) with no frequency averaging performed. Most of the CLF ratios fluctuated within $\pm$10 dB. Some systematic variations in the CLF ratio are seen in Fig. 6(b), especially below the second cut-on frequency of plate 1 (734 Hz). However, such effects are not seen for most of the combinations indicated in Table 1.

From plots such as Figs. 4 and 6, the variance, σ^2, of all values is found of the logarithmic ratio of the frequency-averaged effective CLF to the ensemble average CLF. These variances are plotted against the average number of modes per band for the source plate N_{source} or the receiver plate $N_{receiver}$, in Fig. 7(a). The results with no frequency averaging are plotted against the modal overlap factor for the source plate M_{source} or the receiver plate $M_{receiver}$, in Fig. 7(b). No clear trend can be seen from these results, although σ^2 tends to fall with increasing N or M.

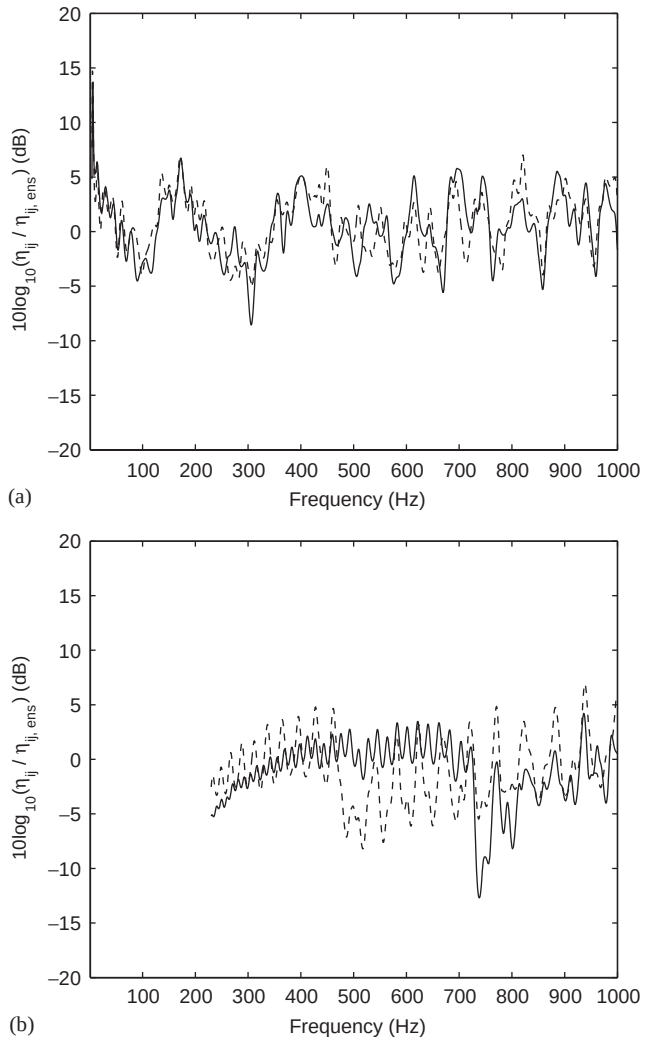

Fig. 6. The logarithmic CLF ratio $10\log_{10}(\hat{\eta}_{ij}/\eta_{ij,ens})$ for two extreme cases; (a) the shortest and widest, (b) the longest and narrowest, when no frequency averaging is performed. —, $10\log_{10}(\hat{\eta}_{12}/\eta_{12,ens})$; - - -, $10\log_{10}(\hat{\eta}_{21}/\eta_{21,ens})$.

Next the results for σ^2 are plotted against $N_{12} = \sqrt{N_1 N_2}$ (the geometric mean number of modes per band), as shown in Fig. 8(a). These results are slightly less scattered than in the previous plots, Fig. 7(a). This result shows that the variance of the CLF has a non-linear relationship with N_{12} on log–log axes. The results for low bandwidth tend to a constant, independent of N_{12}. The results for σ^2 are shown for the cases with no frequency averaging in Fig. 8(b). These represent the limiting case for low N_{12}. They are plotted against $M_{12} = \sqrt{M_1 M_2}$ (the geometric mean modal overlap factor) as used by Mohammed [10]. These non-frequency averaged results show approximately a linear relationship with M_{12} on log–log axes; from the slope of this relationship it is found that σ^2 is inversely proportional to M_{12} for no frequency averaging.

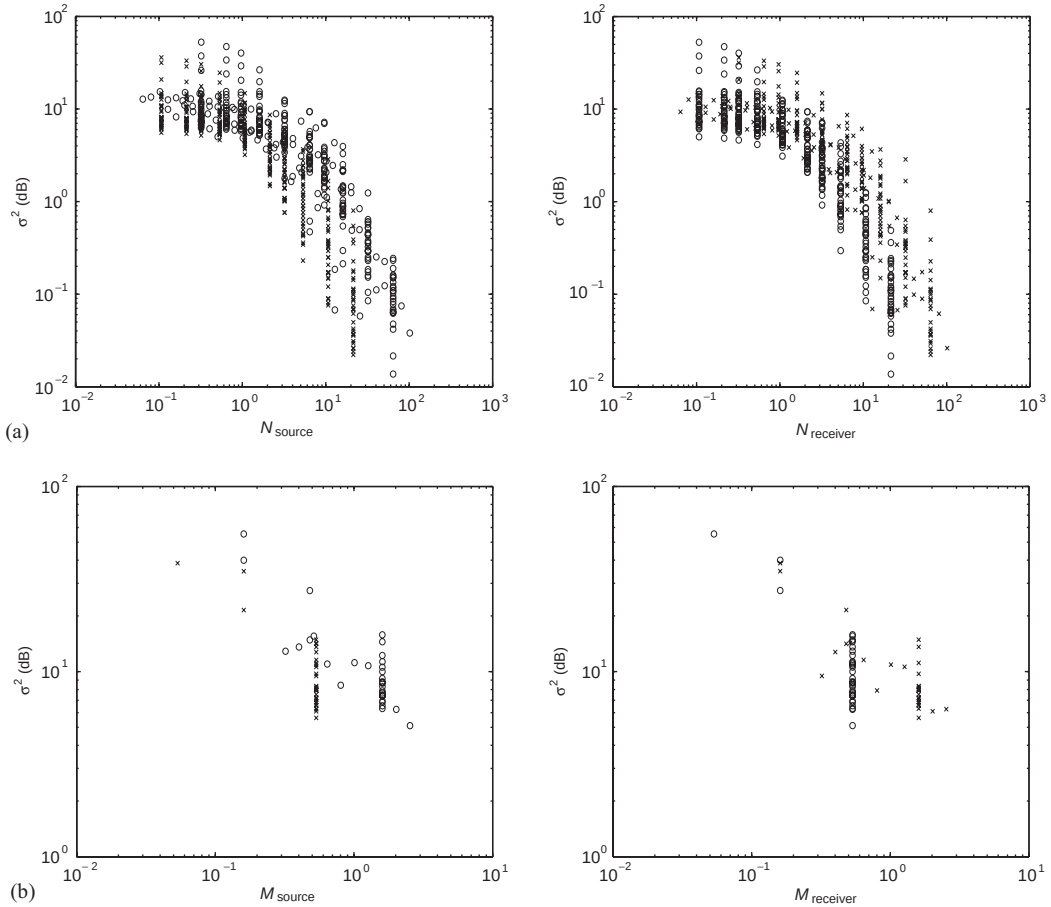

Fig. 7. σ^2 of $10\log_{10}(\langle\hat{\eta}_{ij}\rangle/\eta_{ens})$ for all sets of data plotted against (a) N_{source} and $N_{receiver}$ when the effective CLFs are averaged over frequency bands (2, 4, 6, 10, 20, 40, 60, 100, 200 and 400 Hz) and (b) M_{source} and $M_{receiver}$ when no frequency averaging is performed. Crosses denote results for η_{12} and circles denote those for η_{21}.

The values of σ^2 for low N_{12} are independent of N_{12} and are thus similar to those for no frequency averaging. By multiplying all data points in Fig. 8(a) by M_{12}, the results collapse to a similar level at low values of N_{12}. However, it is also found necessary to shift the points horizontally by a factor of $1/\sqrt{M_{12}}$ to collapse them to a single data set.

The result is shown in Fig. 9 in which $\sigma^2 M_{12}$ is plotted against N_{12}^2/M_{12}.

3.3. 'Combined' modal overlap factor

In order to apply the above concepts to the results for an infinite plate coupled to a finite plate or a finite plate coupled to an infinite plate, the two parameters, M_{12} and N_{12}, cannot be used since the number of modes and modal densities for an infinite plate tend to infinity. Nevertheless it is found in Ref. [21] that the CLF is still affected by the modal behaviour of the finite plate, so that σ^2 does not become zero.

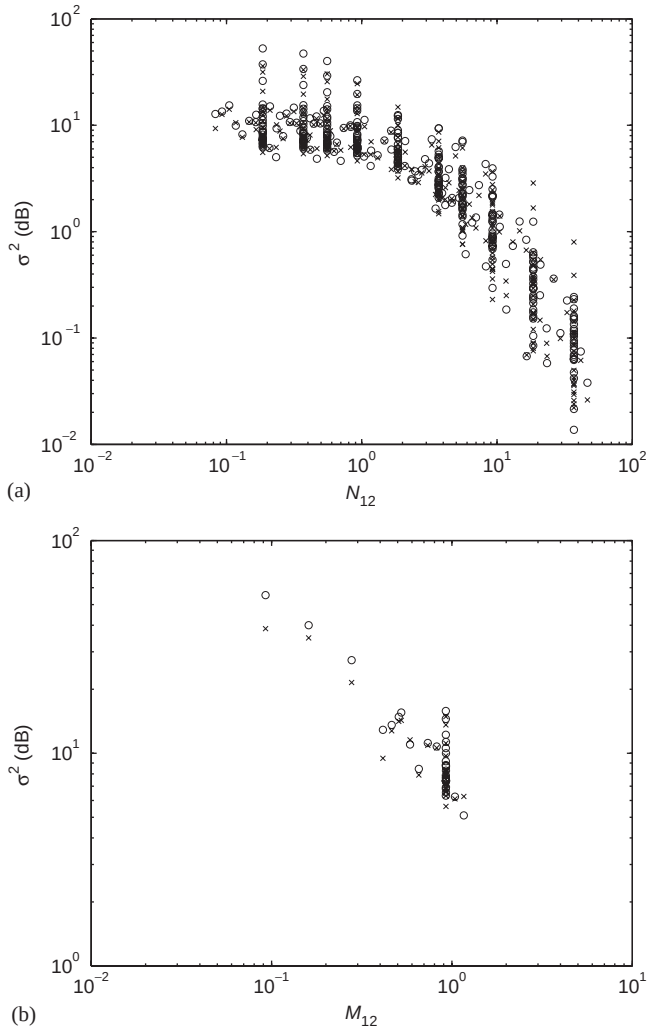

Fig. 8. σ^2 of $10\log_{10}(\langle\hat{\eta}_{ij}\rangle/\eta_{ens})$ for all sets of data plotted against: (a) N_{12} when the effective CLFs are averaged over frequency bands (2, 4, 6, 10, 20, 40, 60, 100, 200 and 400 Hz) and, (b) M_{12} when no frequency averaging is performed. Crosses denote results for η_{12} and circles denote those for η_{21}.

A new 'combined' modal overlap factor is therefore proposed, given by

$$M_{comb} = \frac{2M_1M_2}{M_1 + M_2} = 2\left(\frac{1}{M_1} + \frac{1}{M_2}\right)^{-1}. \tag{2}$$

It may be noted that this satisfies $M_{comb} \approx M_{12}$ for $M_1 \approx M_2$, $M_{comb} = 2\,M_1$ for $M_2 \to \infty$, and $M_{comb} = 2\,M_2$ for $M_1 \to \infty$.

Similarly a new 'combined' number of modes in a band is proposed, given by

$$N_{comb} = \frac{2N_1N_2}{N_1 + N_2} = 2\left(\frac{1}{N_1} + \frac{1}{N_2}\right)^{-1} \tag{3}$$

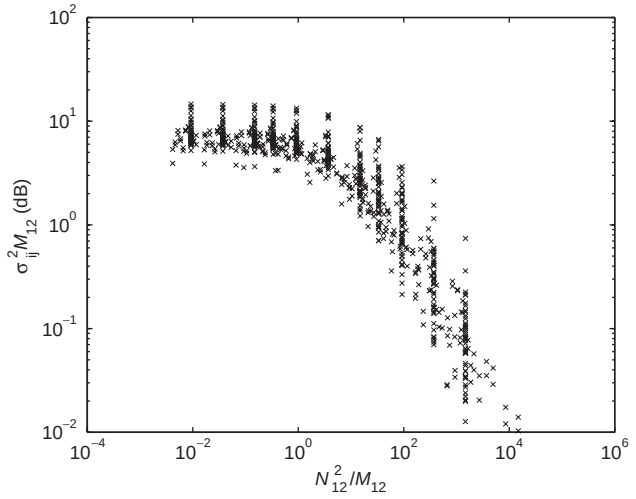

Fig. 9. $\sigma^2 M_{12}$ plotted against N_{12}^2/M_{12}.

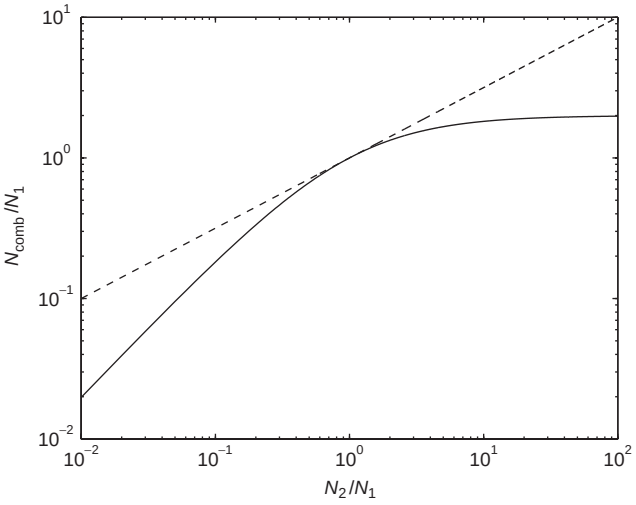

Fig. 10. N_{comb}/N_1 and N_{12}/N_1 plotted against N_2/N_1. —, N_{comb}/N_1; - - -, N_{12}/N_1.

which satisfies $N_{comb} \approx N_{12}$ for $N_1 \approx N_2$, $N_{comb} = 2\,N_1$ for $N_2 \to \infty$, and $N_{comb} = 2\,N_2$ for $N_1 \to \infty$. Eqs. (2) and (3) reflect the fact that the smaller of the two values of N or M dominates the variability of the CLF.

Fig. 10 shows N_{comb}/N_1 plotted against N_2/N_1. This is compared with N_{12}/N_1. This plot shows that the two values N_{comb} and N_{12} are close when $N_1 \sim N_2$. The values of N_2/N_1 and M_2/M_1 considered in the parameter variations in Section 3.1 are limited to the range 0.6–4.7.

3.4. Empirical model for the variability of the CLF

The variance results for all parameter variations are plotted in Fig. 11 in a similar form to Fig. 9 but now $\sigma^2 M_{comb}$ is plotted against N_{comb}^2/M_{comb}. A formula has been established to fit three curves to the data in Fig. 11:

$$\sigma^2 M_{comb} = \frac{a}{(1 + bN_{comb}^2/M_{comb})}, \tag{4}$$

where a and b are constants for the three curves. Dividing through by M_{comb} these can also be expressed in the form

$$\sigma^2 = \frac{a}{(M_{comb} + bN_{comb}^2)}. \tag{5}$$

The dashed and dash-dotted curves have been fitted approximately as the minima and maxima of the ordinate value $\sigma^2 M_{comb}$ as a function of N_{comb}^2/M_{comb} while the solid curve corresponds to a line roughly through the centre of the data. The values of a and b are listed in Table 2. These curves are empirical in the sense that they are obtained by fitting simple curves to the numerical

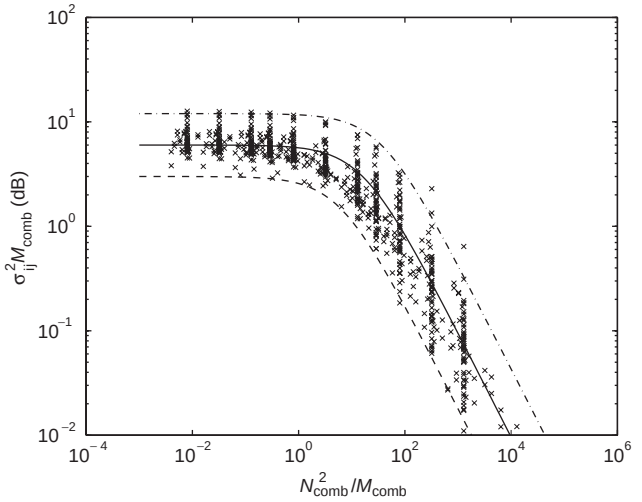

Fig. 11. $\sigma^2 M_{comb}$ plotted against N_{comb}^2/M_{comb} and three curves produced to quantify the variability of the CLF. – · –, $\sigma^2 = 12/(M_{comb} + N_{comb}^2/36)$; —, $\sigma^2 = 6/(M_{comb} + N_{comb}^2/16)$; - - -, $\sigma^2 = 3/(M_{comb} + N_{comb}^2/6)$.

Table 2
Percentage of points falling within $\pm 2\sigma$ limits defined by Eq. (5) $\sigma^2 = a/(M_{comb} + bN_{comb}^2)$ for all sets of data

a	b	Confidence interval (%)
3	$\frac{1}{6}$	73.4
6	$\frac{1}{16}$	95.7
12	$\frac{1}{36}$	99.2

results, not obtained directly by theoretical considerations. The word empirical is often used to refer to experimental data but this is not the case here.

Using each of these curves rather than the original data points, a predicted confidence interval ($\pm 2\sigma$) for $10\log_{10}(\langle\hat{\eta}\rangle/\eta_{ens})$ has been determined for each pair of plates represented and each frequency bandwidth. In each case, by comparing the DSM predictions with this predicted confidence interval, the percentage of frequency points falling inside this interval has been determined. Taking the average over all plates considered, the confidence level represented by each of the formulae was determined and is given in Table 2. Of these, the second curve is adopted as the 'empirical model' for the variability of the CLF:

$$\sigma^2 = \frac{6}{(M_{comb} + N_{comb}^2/16)}. \tag{6}$$

The value of $\pm 2\sigma$ from this formula represents a 95.7% confidence interval for all sets of data considered. This model can be generally used to evaluate the uncertainty of the CLF of a two-coupled plate system. It can also be used to cover situations where one plate is effectively infinite. However it should be noted that the model fails if the plates are very narrow (Fig. 6(b)) or very wide. In the latter case N_{comb} will become large but variability will remain.

3.5. Comparison with previously published models

The current results, displayed in Fig. 11, have been converted into the form used in Mohammed's model [10] and are plotted in Fig. 12. A straight line of best fit is also given. It will be noted that this does not have a slope of -1 as suggested by Mohammed (shown as a dashed line). This indicates, instead, that the normalized variance is proportional to $M_{12}^{-0.60}N_{12}^{-0.58}$. This

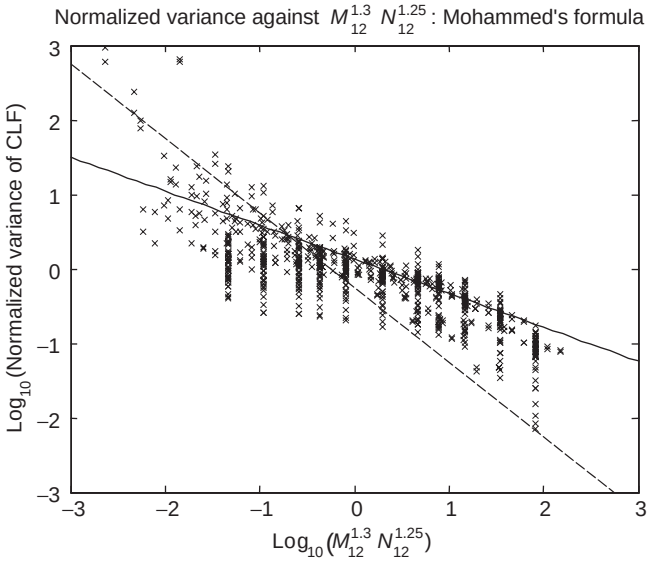

Fig. 12. The normalized variance $\sigma^2/\langle\hat{\eta}_{ij}\rangle$ plotted against $(M_{12})^{1.3}(N_{12})^{1.25}$ on log–log axes based on Mohammed's formula [10]. The straight line of slope –0.46 and intercept 0.13 (—) is the best straight line fit through the log–log data values. The line of slope –1 (- - -) corresponds to Mohammed's model.

graph shows that the current results, based on a data set that far exceeds the number of configurations previously used, cannot be well represented by a simple straight line, as suggested by Mohammed [10]. The present model seems more appropriate as it depends on the number of modes in the band where this is large but is more sensitive to the modal overlap where there are fewer modes.

In order to compare the present model with various previously published models for the variability in CLF estimates, the predicted standard deviation is plotted against the actual standard deviation for all cases considered in the parameter study of this section. Fig. 13(a) gives the results for the present model which can be seen to lie close to the ideal straight line.

The model of Craik et al. [6] has two different estimates for the 'upper bound', one based on a single mode, the other based on multiple modes in a frequency band. These are plotted in Figs. 13(b) and (c). The first of these is based on the modal overlap factor whereas the second is

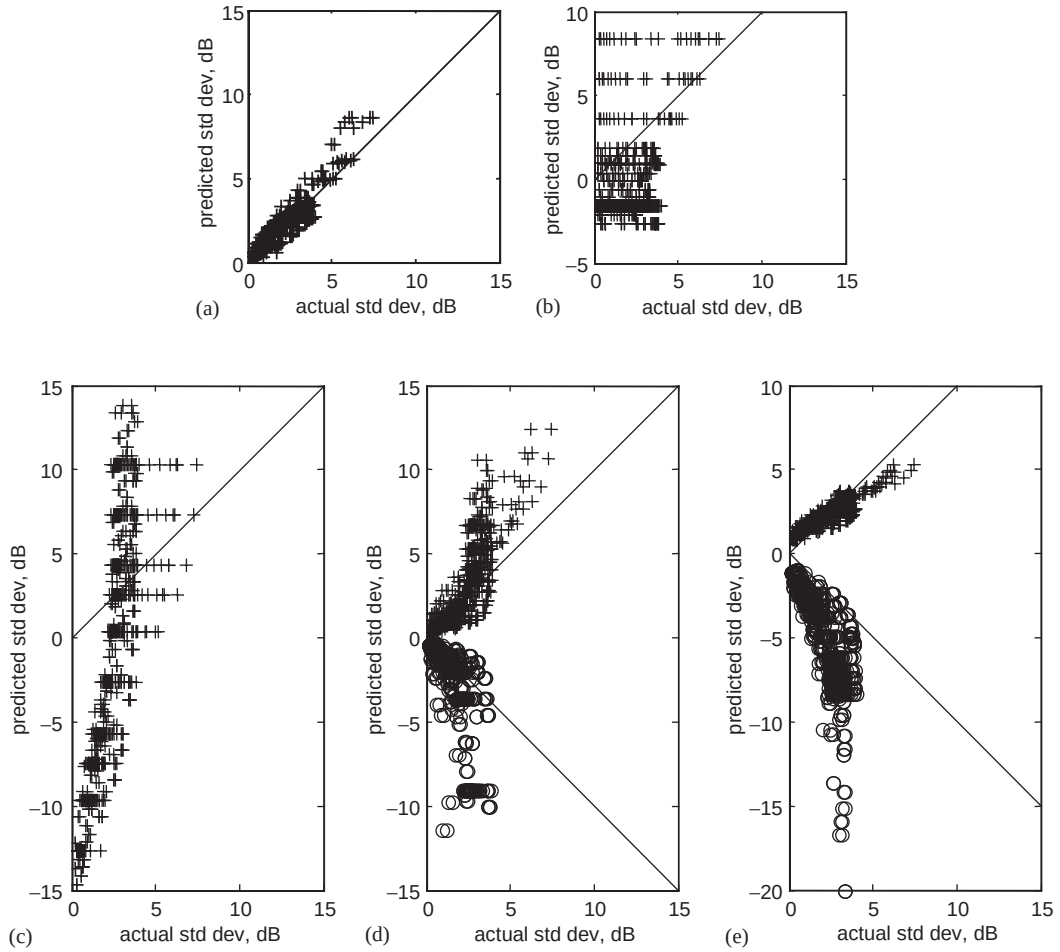

Fig. 13. Comparison between actual standard deviations and those predicted by various models. (a) Present model, (b) Craik et al. [6] (upper bound based on single mode), (c) Craik et al. [6] (upper bound based on multiple modes), (d) Mohammed [10], (e) Lyon and DeJong [5].

based on the number of modes in a band. Clearly neither parameter is sufficient to determine the variability. In these figures, especially for the multiple mode case, the upper bound plotted actually falls below the mean value for high modal overlap or a large number of modes in the band. The model would effectively predict a variance of zero in these cases, when the actual standard deviation is non-zero.

Results for the models of Mohammed [10] and Lyon and DeJong [5] are plotted in Fig. 13(d) and (e). These models are based on the normalized variance of the CLF rather than the standard deviation of the logarithmic CLF. Thus the region of ± 1 standard deviation is not symmetric when plotted on a decibel scale. The values at ± 1 standard deviation are plotted in the figure using different symbols to indicate the upper and lower 'bounds' from the two models [10,5]. When the standard deviation exceeds the mean, the lower limit becomes infinite. Strictly such a distribution is not normal so that the 68% confidence interval is not simply $\pm\sigma$. However this has not been pursued further here.

It can be seen from Fig. 13 that the current model gives much better agreement with the actual standard deviations calculated using the DSM model than any of the previously published models. Lyon and DeJong is the closest of the others, although it over-predicts the variance for small standard deviations, and over-predicts the range ± 1 standard deviation in all cases.

Applying the model developed in this paper to the cases covered in Section 2.1 leads to the results shown in Fig. 14. The upper and lower bounds of the logarithmic CLF ratio $10\log_{10}(\langle\hat{\eta}_{12}\rangle/\eta_{12,ens})$ found are rather large at low frequencies, especially for the lower damping value. Here, however, the combined modal overlap factor M_{comb} falls well outside the range 0.1–1 that was used to generate the empirical model (see Fig. 8(b)). For the higher value of damping loss factor, $M_{comb}<0.1$ for frequencies below 12.5 Hz; for the lower damping value this occurs for frequencies below 125 Hz. In these frequency regions the model over-predicts the bounds. This suggests that the present empirical model should not be used for modal overlap factors less than about 0.1. Further calculations would be necessary to extend the range of the model to lower values of M. In practice, however, the level of variability obtained for such low values of modal overlap (95% confidence intervals of more than about ± 10 dB) render an SEA-type calculation unacceptable in such situations anyway.

3.6. *Interdependence of CLF*s

In the empirical model above, the variability of η_{12} and η_{21} has been considered without regard to their interdependence. In this section, the degree to which the two variables, η_{12} and η_{21}, are linearly related is investigated. For this purpose, a normalized variance ratio is defined by $\sigma_d^2/(\sigma_{12}\sigma_{21})$, where σ_d^2 is the variance of the difference between $10\log_{10}(\langle\hat{\eta}_{21}\rangle/\eta_{21,ens})$ and $10\log_{10}(\langle\hat{\eta}_{12}\rangle/\eta_{12,ens})$ and σ_{12} and σ_{21} are the standard deviations of the two logarithmic CLF ratios, respectively. The normalized variance ratio for all datasets is shown in Fig. 15(a). When they are dependent on each other the variance ratios should lie well below 1 but in some cases they are greater than 1. Another parameter that can be used is the correlation coefficient [22]. The correlation coefficient is a non-dimensional number that lies between –1 and +1. Most of the correlation coefficients in Fig. 15(b) are positive and close to unity indicating that in these situations η_{12} and η_{21} are well correlated. In summary, in 89.1% of all cases considered the absolute value of the correlation coefficient is greater than and equal to 0.5. The cases with poor

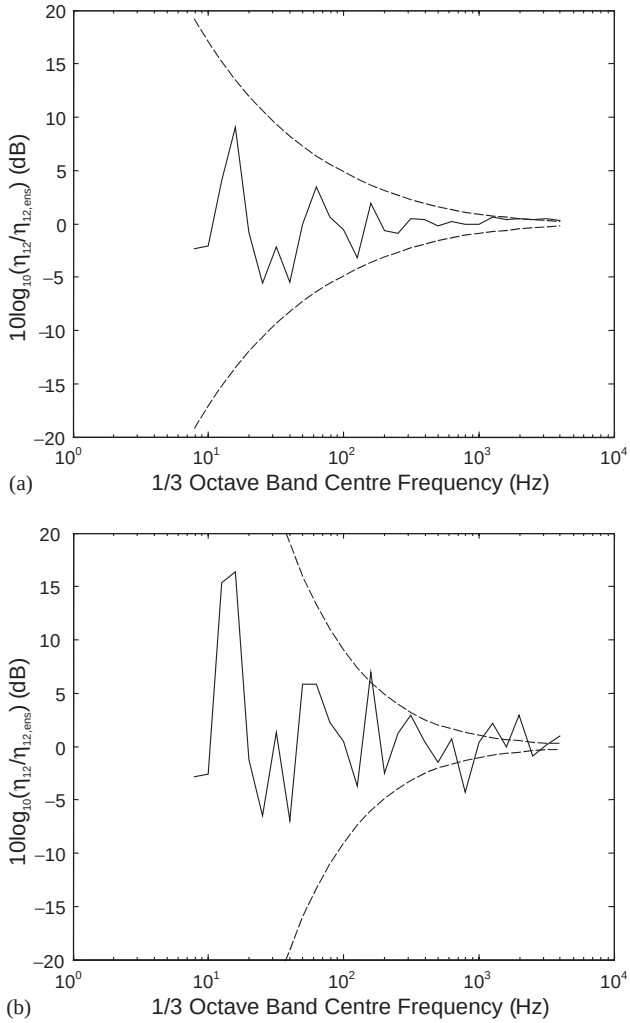

Fig. 14. Logarithmic CLF ratio $10\log_{10}(\langle\hat{\eta}_{12}\rangle/\eta_{12,ens})$ for the initial model obtained from the DSM and the $\pm 2\sigma$ estimate obtained from Eq. (6). (a) $\eta = 0.1$, (b) $\eta = 0.01$. —, DSM result; - - - from Eq. (6).

correlation are mostly long narrow plates. This actually indicates a problem with the ensemble average CLF used $\eta_{ij,ens}$ rather than the independence of η_{12} and η_{21} (see Fig. 6(b)). It may be noted that these plates are very narrow and are effectively one dimensional at low frequencies. Here the results based on $\eta_{ij,ens}$ are not appropriate.

4. Concluding remarks

In this paper, the variability of the CLF for a system of two coupled rectangular plates has been examined and quantified using a systematic parameter variation. The ensemble average CLF

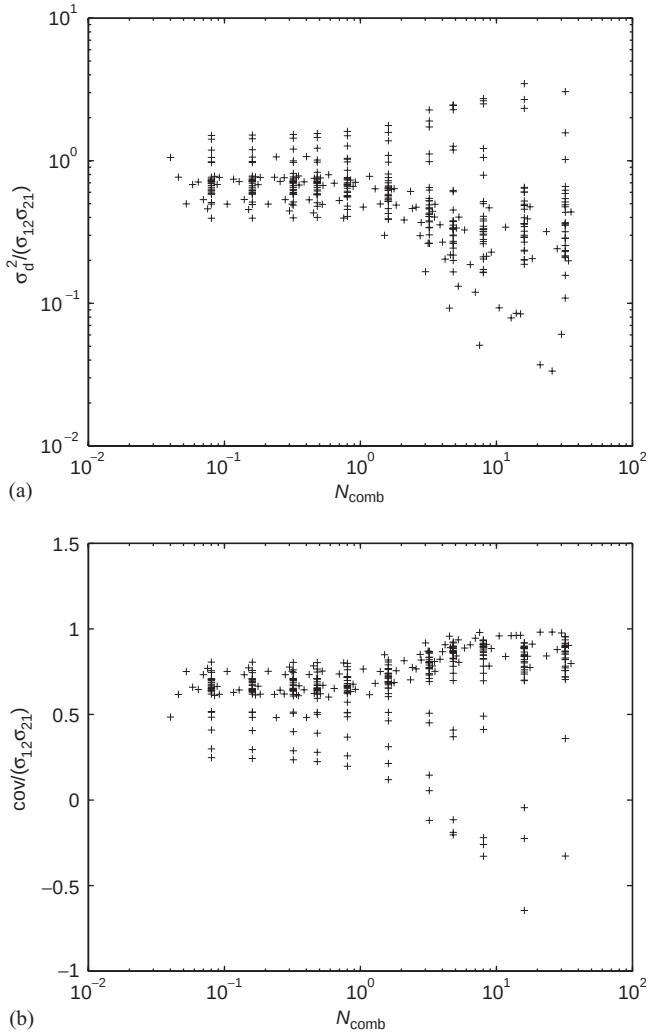

Fig. 15. (a) The variance ratio for all cases of parameter variations plotted against N_{comb} and (b) the correlation coefficient plotted against N_{comb}.

given by Wester and Mace [15] was used as an unbiased estimate of the average CLF for all cases, providing a good basis for studying the variability. An empirical model for the variability of the CLF has been developed using these results.

Firstly, narrow band energies and powers were calculated for a large number of configurations using the dynamic stiffness method. The modal overlap factor was kept constant versus frequency by using a loss factor that was inversely proportional to frequency. The effective CLFs $\langle \hat{\eta}_{ij} \rangle$ were obtained from these energies averaged over frequency bands. The effects of frequency and modal overlap were separated by using frequency averages at a series of constant bandwidths rather than one-third octave averages.

Secondly, the logarithmic ratio of the effective CLF to the ensemble average, $10 \log_{10}(\langle \hat{\eta}_{ij} \rangle / \eta_{ij,ens})$, was determined and the variance σ^2 was obtained over the whole frequency

region for each case to express the variability of the effective CLF compared with the ensemble average. An empirical model was developed to express the dependence of the variance σ^2 on the modal overlap factors and numbers of modes in a frequency band. For small numbers of modes in a band the modal overlap has the dominant effect, but for large numbers of modes in a band it is this number that has the dominant effect.

The model should not be used for very narrow plates nor for extremely wide plates. For modal overlap factors less than 0.1, it is observed that the empirical model gives overestimates of the variance. However, for such low modal overlap factors, the variance is in any case too large for practical use of SEA-type models.

This model has been developed for a system of two coupled rectangular plates and can be used to evaluate the uncertainty of the CLF of that system. However it is not certain whether other types of system can be represented by the same model. This should be the subject of further research.

Acknowledgements

The authors are grateful to Dr. Brian Mace for helpful suggestions and discussions. The first author gratefully acknowledges the financial support provided by the British Chevening Scholarship and Daewoo Motor Company.

Appendix

From Ref. [15], the diffuse field coupling loss factor between two edge coupled simply supported plates is given by

$$\eta_\infty = \frac{2\overline{T^2}}{\pi k_i l_i},$$

where T is the magnitude of the transmission coefficient for a particular angle of incidence, k_i the free wavenumber in the source plate, and l_i the length of the source plate. The plates have common width. The exact ensemble average CLF for the plates is then given by Ref. [15] as

$$\eta_{ij} = \eta_\infty \Big/ \left[\left(\frac{1}{k_i} \int_0^{\min(k_i,k_j)} \frac{T^2(k_y)/\overline{T^2}}{\sqrt{1+\gamma^2(k_y)}\sqrt{1+\delta^2(k_y)}} \, \mathrm{d}k_y \right)^{-1} - \frac{\overline{T^2}}{\pi\mu_{i0}} \left(1 + \frac{k_i\mu_{i0}}{k_j\mu_{j0}} \right) \right],$$

where the terms are described in detail in Ref. [15]. k_y is the trace wavenumber along the connection and k_i and k_j the free wavenumbers in the two plates. $\mu_{i0} = k_i l_i \eta_i/2$ and $\mu_{j0} = k_j l_j \eta_j/2$ are the limiting subsystem 'reflectances' for small trace wavenumber k_y, γ, δ are strength of coupling parameters given by

$$\gamma^2 = \frac{T^2\cosh^2(\mu_d)}{\sinh(\mu_a)\sinh(\mu_b)} \quad \text{and} \quad \delta^2 = \frac{T^2\sinh^2(\mu_d)}{\sinh(\mu_a)\sinh(\mu_b)},$$

where $\mu_i \approx \mu_{i0}/\sqrt{1-(k_y/k_i)^2}$, $\mu_j \approx \mu_{j0}/\sqrt{1-(k_y/k_j)^2}$ and $\mu_d = (\mu_i - \mu_j)/2$.

References

[1] M. Heckl, M. Lewit, Statistical energy analysis as a tool for quantifying sound and vibration transmission paths, in: A.J. Keane, W.G. Price (Eds.), *Statistical Energy Analysis*; *an Overview*, *with Applications in Structural Dynamics*, Cambridge, University Press, Cambridge, 1997, pp. 19–34, (Originally published in Philosophical Transactions of the Royal Society of London Series A 346 (1994) 429–554).

[2] G. Borello, Prediction and control of structure borne noise transfers in vehicles using SEA, *Proceedings of Euro-Noise 98*, Munich, Germany; 1998, pp. 183–188.

[3] P. Hynna, P. Klinge, J. Vuoksinen, Prediction of structure-borne sound transmission in large welded ship structures using statistical energy analysis, *Journal of Sound and Vibration* 180 (4) (1995) 583–607.

[4] B.M. Gibbs, C.L.S. Gilford, The use of power flow methods for the assessment of sound transmission in building structures, *Journal of Sound and Vibration* 49 (2) (1976) 267–286.

[5] R.H. Lyon, R.G. DeJong, *Theory and Application of Statistical Energy Analysis*, 2nd Edition, Butterworth-Heinemann, Boston, 1995.

[6] R.J.M. Craik, J.A. Steel, D.I. Evans, Statistical energy analysis of structure-borne sound transmission at low frequencies, *Journal of Sound and Vibration* 144 (1) (1991) 95–107.

[7] E. Skudrzyk, The mean-value method of predicting the dynamic response of complex vibrations, *Journal of the Acoustical Society of America* 67 (4) (1980) 1105–1135.

[8] A.T. Moorhouse, B.M. Gibbs, Calculation of the mean and maximum mobility for concrete floors, *Applied Acoustics* 45 (1995) 227–245.

[9] F.J. Fahy, A.D. Mohammed, A study of uncertainty in application of SEA to coupled beam and plate systems, Part I: computational experiments, *Journal of Sound and Vibration* 158 (1) (1992) 45–67.

[10] A.D. Mohammed, A study of uncertainty in applications of statistical energy analysis, Ph.D. Thesis, University of Southampton, Southampton, UK, 1990.

[11] J.E. Manning, Confidence intervals for SEA model predictions, *NOISE-CON 98*, Ypsilanti, Michigan, 1998, pp. 599–604.

[12] C. Hopkins, Statistical energy analysis of coupled plate systems with low modal density and low modal overlap, *Journal of Sound and Vibration* 251 (2) (2002) 193–214.

[13] R.S. Langley, Application of the dynamic stiffness method to the free and forced vibrations of aircraft panels, *Journal of Sound and Vibration* 135 (2) (1989) 319–331.

[14] D.A. Bies, S. Hamid, In situ determination of loss and coupling loss factors by the power injection method, *Journal of Sound and Vibration* 70 (2) (1980) 187–204.

[15] E.C.N. Wester, B.R. Mace, Statistical energy analysis of two edge-coupled rectangular plates: ensemble averages, *Journal of Sound and Vibration* 193 (4) (1996) 793–822.

[16] D.G. Crighton, A.P. Dowling, J.E. Ffowcs Williams, M. Heckl, F.G. Leppington, *Modern Methods in Analytical Acoustics*, Springer, London, 1992, p. 258.

[17] L. Cremer, M. Heckl, E.E. Ungar, *Structure-Borne Sound*, 2nd Edition, Springer, New York, 1988.

[18] F.J. Fahy, Statistical energy analysis: a wolf in sheep's clothing? *Proceedings of Internoise 93*, Leuven, 1993, pp. 13–26.

[19] R.J.M. Craik, *Sound Transmission through Buildings using Statistical Energy Analysis*, Aldershot, Gower, 1996.

[20] B.R. Mace, The statistical energy analysis of two continuous one-dimensional subsystems, *Journal of Sound and Vibration* 166 (3) (1993) 429–461.

[21] W.S. Park, D.J. Thompson, N.S. Ferguson, The influence of the modal behaviour on the energy transmission between two coupled plates, *Journal of Sound and Vibration* 276 (3–5) (2004) 1019–1041.

[22] G.W. Snedecor, W.G. Cochran, *Statistical Methods*, 6th Edition, The Iowa State University Press, Ames, Iowa, 1967.